Geophysical Research Letters

RESEARCH LETTER
10.1029/2023GL104137

Anomalously Darker Land Surfaces Become Wetter Due To Mesoscale Circulations

Yu Cheng[1], **Zeyuan Hu**[1], **and Kaighin A. McColl**[1,2]

[1]Department of Earth and Planetary Sciences, Harvard University, Cambridge, MA, USA, [2]School of Engineering and Applied Sciences, Harvard University, Cambridge, MA, USA

Key Points:

- Land radiative management (LRM)—increasing land surface albedo to reduce temperatures—has been proposed as a form of geoengineering
- We use idealized cloud-permitting simulations and a conceptual model to understand the hydrologic response to LRM
- LRM increases rainfall and soil moisture in surrounding regions, potentially extending its cooling benefits

Supporting Information:

Supporting Information may be found in the online version of this article.

Correspondence to:

K. A. McColl,
kmccoll@seas.harvard.edu

Citation:

Cheng, Y., Hu, Z., & McColl, K. A. (2023). Anomalously darker land surfaces become wetter due to mesoscale circulations. *Geophysical Research Letters*, *50*, e2023GL104137. https://doi.org/10.1029/2023GL104137

Received 14 APR 2023
Accepted 28 AUG 2023

Abstract

"Land radiative management" (LRM)—intentionally increasing land surface albedo to reduce regional temperatures—has been proposed as a form of geoengineering. Its effects on local precipitation and soil moisture over long timescales are not well understood. We use idealized cloud-permitting simulations and a conceptual model to understand the response of precipitation and soil moisture to a mesoscale albedo anomaly at equilibrium. Initially, differential heating between a high-albedo anomaly and the lower-albedo surrounding environment drives mesoscale circulations, increasing precipitation and soil moisture in the surrounding environment. However, over time, increasing soil moisture reduces the differential heating, eliminating the mesoscale circulations. At equilibrium, the fractional increase in simulated soil moisture is up to 1.3 times the fractional increase in co-albedo (one minus albedo). Thus, LRM may increase precipitation and soil moisture in surrounding regions, enhancing evaporative cooling and spreading the benefits of LRM over a wider region than previously recognized.

Plain Language Summary

One way to reduce temperatures in a warming world is to increase the fraction of sunlight reflected by the land surface back to space (the "albedo"), for example, by painting surfaces white. However, changing albedo does not only change temperatures; it can also impact rainfall and soil moisture. Here, we show that increasing a region's albedo leads to increased rainfall and soil moisture in surrounding regions, where the albedo has not been changed, spreading the cooling effect over a wider area than previously recognized.

1. Introduction

The impacts of spatial variability in land surface albedo on precipitation have been widely studied at global and regional scales (e.g., Charney (1975), Charney et al. (1977), Davin and Noblet-Ducoudré (2010), Laguë et al. (2019), and Tang et al. (2023)). At mesoscales (O(10 km)), many studies have examined the impacts of an albedo anomaly on precipitation in the context of deforestation (Chagnon & Bras, 2005; Negri et al., 2004; Taylor et al., 2022; Wang et al., 2000), which causes coincident anomalies in albedo, surface roughness, and vegetation. Others have also examined the transient (hours to days) creation of mesoscale circulations in response to albedo anomalies corresponding to salt lakes (Physick & Tapper, 1990; Tapper, 1991) or other geological formations (Pielke et al., 1993), although they do not explicitly assess the precipitation response.

Remarkably, to our knowledge, no studies have examined the *equilibrium* (months or longer) precipitation response to a *mesoscale* albedo anomaly *in isolation*, that is, without coincident anomalies in surface roughness or other land surface properties (see Figure S1 in Supporting Information S1 for an overview of how this study relates to previous literature (Charney, 1975; Devaraju et al., 2015; Evans et al., 2017; Hales et al., 2004; Li et al., 2018; Mostamandi et al., 2022; Oleson et al., 2010; Ouyang et al., 2022; Physick & Tapper, 1990; Sharma et al., 2016; Taylor et al., 2022; Vahmani et al., 2016; Wang et al., 2000; Xue & Shukla, 1993; Zonato et al., 2021)). This response is of fundamental interest, but also has important practical relevance. Recent proposals for land radiative management (LRM)—a form of local geoengineering—specifically focus on modifying landscape albedo at mesoscales to reduce temperatures (Seneviratne et al., 2018). In agricultural areas, the proposed approaches include no-till farming (Davin et al., 2014) and bioengineered modification of crop albedo (Genesio et al., 2021). In urban areas, the use of white roofs and reflective pavements has also been proposed. Such approaches are capable of causing changes in surface albedo of up to 0.15 (summarized in Table 1 of Seneviratne et al. (2018)) in the shortwave band (approximately 0.3–5 μm), while minimally changing other land surface variables. Although not widespread today, it is plausible that such techniques may be deployed at scales approaching 10 km in future

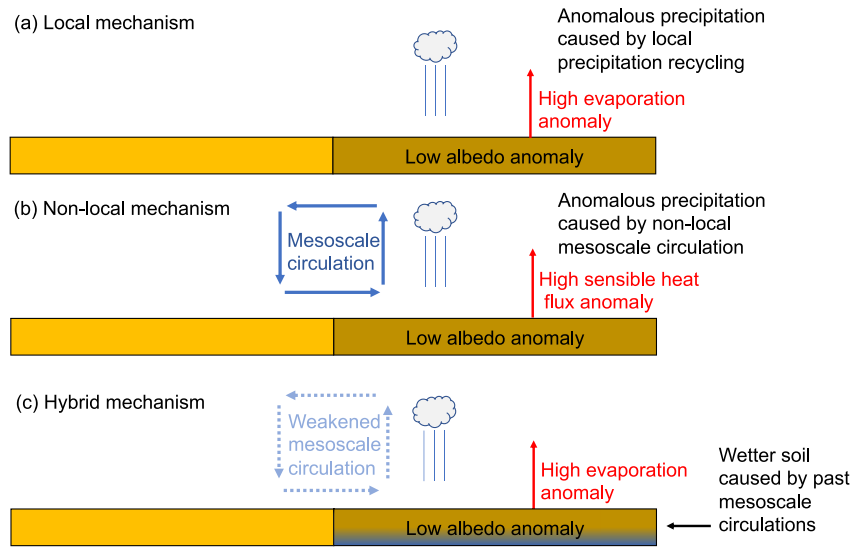

Figure 1. Precipitation responses to anomalously low albedo. (a) A local mechanism, in which anomalously high surface evaporation is recycled into anomalously high precipitation, without changing soil moisture. (b) A non-local mechanism, in which a mesoscale circulation causes anomalously high precipitation, importing moisture from elsewhere and increasing soil moisture with time. (c) A hybrid mechanism, in which the non-local mechanism dominates initially, but wanes with time as soil moisture increases, which decreases the differential heating driving the mesoscale circulation. At equilibrium, the hybrid mechanism differs from both the local and non-local mechanisms. Unlike the local mechanism, soil moisture increases under the hybrid mechanism; unlike the non-local mechanism, there is no longer a significant mesoscale circulation.

in response to global warming. Critically, for many proposed approaches to LRM, the intent is to introduce an albedo anomaly into the landscape *in isolation*, rather than in conjunction with anomalies in surface roughness or vegetation (e.g., vegetation cover and height, leaf area index, stomatal conductance and rooting depth), as is common in studies of deforestation or afforestation.

As we will show, the equilibrium precipitation response to an isolated albedo anomaly differs profoundly from the response to deforestation, in which anomalies in albedo, roughness and vegetation coincide. Consider an idealized environment with a homogeneous land surface, sufficient soil moisture for evaporation to occur, and no mean wind. We highlight two possible mechanisms by which a mesoscale albedo anomaly introduced into this environment could change the local hydrologic cycle. In both cases, an albedo anomaly causes anomalous local net surface radiation. We refer to the first mechanism as the "local" mechanism, in which the net surface radiation anomaly causes an anomalous surface latent heat flux (evaporation of water from land into the atmosphere). The resulting anomalous water vapor is then locally "recycled" into a local precipitation anomaly (Figure 1a). We refer to the second mechanism as the "non-local" mechanism, in which the net surface radiation anomaly causes anomalous surface sensible heat flux and near-surface air temperature. In turn, this causes an anomalous horizontal pressure gradient at the surface that drives a mesoscale circulation (Segal & Arritt, 1992), with anomalously high precipitation caused by the ascending branch of the circulation (Figure 1b) (Note that the mesoscale circulations investigated in this study are driven by differential heating rather than heterogeneity in surface friction, such as those studied in Samuelsson and Tjernström (2001) and Khanna and Medvigy (2014)). For both mechanisms, an anomalously lower albedo results in higher precipitation over the albedo anomaly, given a sufficient supply of moisture. However, there is an important distinction between these two mechanisms. The non-local mechanism causes an anomalously lower albedo land surface to import additional water vapor from surrounding regions, resulting in anomalously higher soil moisture. In contrast, the local mechanism simply recycles existing water, resulting in no change to soil moisture. In other words, the non-local mechanism causes anomalously darker land surfaces to become wetter, whereas the local mechanism does not. Which mechanism dominates, in general? This study aims to answer that question.

Much of the previous work relevant to this question has focused on deforestation, a common cause of albedo anomalies. Studies using regional climate models (RCMs) and satellite observations typically implicate the non-local mechanism in increases in precipitation over deforested regions at scales of O(10 km) (Chagnon &

Bras, 2005; Negri et al., 2004; Taylor et al., 2022; Wang et al., 2000). However, while these studies have provided useful insights, they are limited in understanding the precipitation response to an albedo anomaly in at least two respects.

First, deforestation does not only cause an albedo anomaly; it also causes anomalies in surface roughness, leaf area index and rooting depth (Spracklen et al., 2018). Each of these anomalies also impacts the differential surface heating that drives the mesoscale circulation. Our goal is to understand the unique impact of an albedo anomaly on precipitation, and these additional effects confound that analysis. To avoid confounding effects, we conduct deliberately idealized cloud-permitting simulations in which only an albedo anomaly is present in an otherwise homogeneous domain. This allows us to cleanly identify and understand mechanisms by which anomalous albedo impacts precipitation.

Second, previous studies typically trade higher model spatial resolution for a shorter model integration time. For example, deforestation experiments last 12 hr in Roy (2009), 3 days in Wang et al. (2000), and 10 days in Hartley et al. (2016). These relatively short integration periods are useful for studying the transient response of the coupled land-atmosphere system to an albedo anomaly, but not the equilibrium response. In general, the transient and equilibrium responses can be profoundly different. For example, the transient response of precipitation to a soil moisture anomaly depends strongly on the arbitrary choice of initial atmospheric profile (Cioni & Hohenegger, 2018). In contrast, the equilibrium response is relatively insensitive to the initial atmospheric profile; instead, the atmospheric state is partially set by the soil moisture anomaly itself, with drier surfaces causing drier atmospheres that reduce precipitation, in general (Cheng et al., 2021). In this study, we are interested in understanding the equilibrium response of precipitation to an albedo anomaly, and thus conduct cloud-permitting simulations over a period of 500 days.

As we will show, the equilibrium response of precipitation to an albedo anomaly differs profoundly from the transient response examined in earlier studies. The transient response is dominated by the non-local mechanism, implying that darker land surfaces receive more precipitation due to mesoscale circulations. However, the additional precipitation accumulates in the soil with time and generates a soil moisture anomaly, which reduces the heating differential driving the mesoscale circulation. At equilibrium, the heating differential caused by the soil moisture anomaly and the albedo anomaly approximately cancel out, resulting in limited net moisture advection by mesoscale circulations. The resulting precipitation response is a hybrid of the local and non-local mechanisms: a soil moisture anomaly is created, which is characteristic of the non-local mechanism, but there is only limited net moisture transport by the mesoscale circulation, which is characteristic of the local mechanism (Figure 1c).

2. Simulations

We perform cloud-permitting simulations over an idealized land surface, similar to that shown in Figure 1, with varied albedo anomalies. Specifically, we use the System for Atmospheric Modeling (SAM (Khairoutdinov & Randall, 2003); version 6.11.1) coupled to a land surface model (Lee & Khairoutdinov, 2015). To ensure albedos remain fixed, we deliberately set soil albedo to be independent of soil moisture (typically, the soil albedo would vary with soil moisture). To reasonably model the interaction between convection and large-scale forcing over a tropical land surface, we use the weak-temperature gradient (WTG) approximation introduced by Sobel et al. (2001). A complete list of experiments performed with different prescribed albedo anomalies and initial soil moisture values are shown in Table S1 in Supporting Information S1. In our numerical experiments, "High" denotes the experiment where the prescribed visible albedo of soil in the two parts of the domain are 0.1425 and 0.0356, respectively. "Medium" denotes the experiment where the prescribed visible albedo of soil in the two parts of the domain are 0.1425 and 0.0713, respectively. "None1" ("None2") denotes the experiment where the prescribed visible albedo of soil in the two parts of the domain are both 0.1425 (0.1069). In addition to the experiments detailed above, we also conducted simulations in which cold pools—density currents generated by cooling from evaporating hydrometeors (Betts & Silva Dias, 1979; Xu & Moncrieff, 1994)—are eliminated as listed in Table S1 in Supporting Information S1, which are referred to as the "NOCP" simulations. Advection by cold pools is a similar but separate mechanism compared to the mesoscale circulations that are our primary focus. The detailed setup of numerical simulations is available in Supporting Information S1 (Abbott & Cronin, 2021; Anber et al., 2015; Cheng & McColl, 2023; Kiehl et al., 1998; Raymond & Zeng, 2005; Rieck et al., 2015; Sessions et al., 2010; Sobel et al., 2007; Zhou et al., 2003).

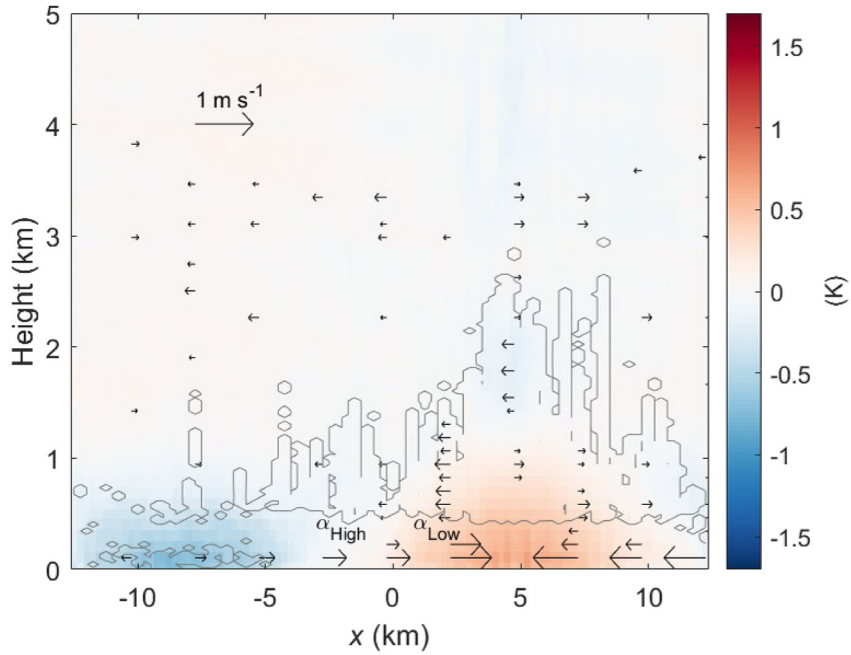

Figure 2. Presence of mesoscale circulations in numerical simulations. *x*-*z* diagram at 9:30 a.m. local time of *y*-averaged quantities for the experiment "Medium" on day 500, where the prescribed visible albedo of soil in the two parts of the domain are 0.1425 and 0.0713, respectively. The color contours denote temperature anomaly. The black arrows denote zonal velocity anomaly, that is, the difference between zonal velocity and its mean at each height. Note that the zonal velocity anomaly is only presented for those with a magnitude greater than 0.1 m s^{-1}. The arrow below "1 m s^{-1}" in the figure is not a real velocity but just used as a reference velocity scale. The gray isolines denote non-precipitating cloud ice and water equal to 10^{-5} g kg^{-1}. The *x* axis denotes the distance from the domain center in *x* direction.

2.1. Presence of Mesoscale Circulations

At equilibrium (Figure S3 in Supporting Information S1), thermally-direct mesoscale circulations (Physick & Tapper, 1990) form in our simulations in the presence of an albedo anomaly, driven by the induced surface sensible heat flux anomaly (Segal & Arritt, 1992). An example is highlighted in Figure 2. At 9:30 a.m. local time on a typical day at equilibrium (day 500 of our simulation), the sensible heat flux over the low albedo anomaly is about 5 W m^{-2} larger than that over the rest of the domain (Figure 2), leading to a temperature anomaly of approximately 0.7 K. The temperature anomaly creates a pressure anomaly of approximately 6 Pa near the surface, which causes horizontal convergence near the surface, rising air and divergence above 1 km over the low albedo anomaly. Clouds form over the low albedo anomaly in response to rising air, which ultimately lead to precipitation. While clouds change the effective albedo of the atmospheric column, these effects are not first-order in explaining the hydrologic response (see Section 3, and Section S1.4.5 in Supporting Information S1).

2.2. Equilibrium Hydrologic Response to Albedo Anomalies

As expected, the low-albedo anomaly causes a positive precipitation anomaly in our simulations, with larger albedo anomalies causing larger precipitation anomalies (denoted by ΔP as shown in Figure 3g, where $\Delta P \equiv P_L - P_H$, P_L is precipitation over the low albedo anomaly, and P_H is precipitation over the relatively higher-albedo patch). The same is true for anomalies in evaporation (denoted by ΔE as shown in Figure 3e) and soil moisture (denoted by $\Delta\phi$ as shown in Figure 3a). In particular, at equilibrium, the fractional increase in simulated soil moisture is 1.3 and 1.1 times the fractional increase in co-albedo (one minus albedo), for simulations "High" and "Medium", respectively. On the other hand, at equilibrium, the heating differential (denoted by ΔH, the sensible heat flux anomaly) that drives mesoscale circulations is small, resulting in a negligible net advection of moisture (denoted by A_L as shown in Figure 3e, where A_L is the net horizontal advection of moisture into the low albedo anomaly). Furthermore, in simulations with an albedo anomaly present, net moisture advection is positive early in the simulation, but decreases with time (Figure 4a). The decline in net moisture advection coincides with declining ΔH (Figure 4b) and rising $\Delta\phi$ (Figure 4c).

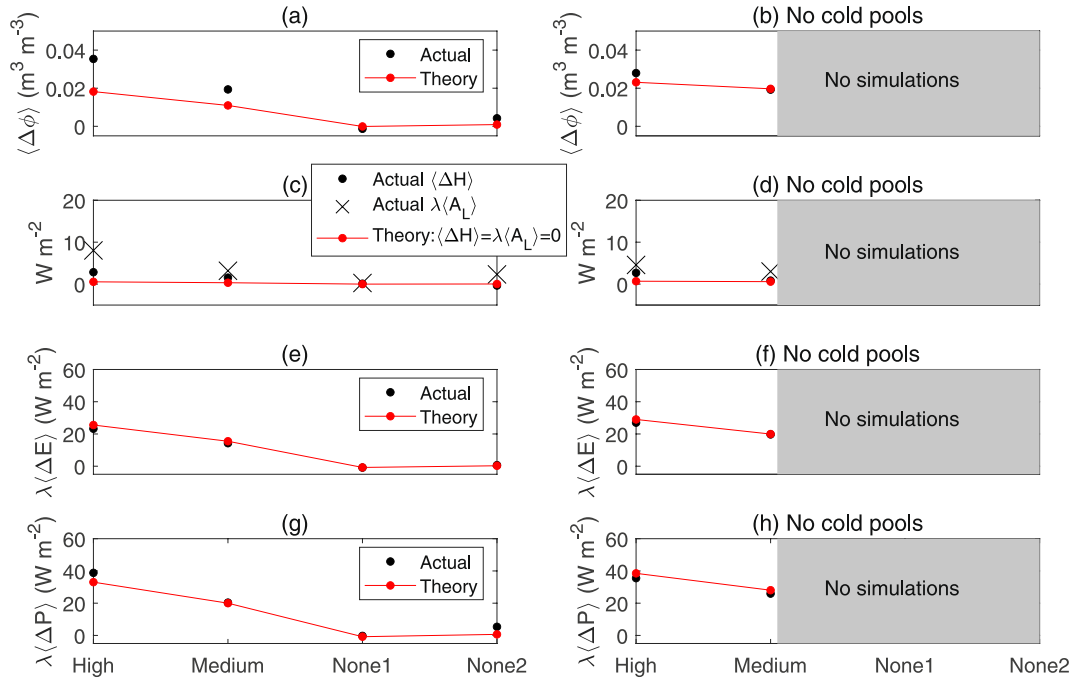

Figure 3. Comparison of cloud-permitting simulation outputs (denoted by "Actual") with predictions from the general conceptual model (Equations S15–S18 in Supporting Information S1; denoted by "Theory"). In panels (b), (d), (f), and (h), the comparison is with simulations in which cold pools were artificially suppressed. The names of numerical experiments are indicated in the *x* axis: "High", "Medium", "None1", and "None2" (Table S1 in Supporting Information S1). "High" denotes the experiment where the prescribed visible albedo of soil in the two parts of the domain are 0.1425 and 0.0356, respectively. "Medium" denotes the experiment where the prescribed visible albedo of soil in the two parts of the domain are 0.1425 and 0.0713, respectively. "None1" ("None2") denotes the experiment where the prescribed visible albedo of soil in the two parts of the domain are both 0.1425 (0.1069). (a) and (b) Soil moisture anomaly ($\Delta\phi$). (c) and (d) Sensible heat flux anomaly (ΔH) and net horizontal advection of moisture into the low albedo anomaly (A_L). (e) and (f) Latent heat flux anomaly ($\lambda\Delta E$). (g) and (h) Precipitation anomaly ($\lambda\Delta P$). Note that the *y*-axis limits in (c) and (d) differ from those in (e)–(h).

These results do not fit neatly with either the local (Figure 1a) or the non-local (Figure 1b) mechanisms described earlier. The fact that net moisture advection is small at equilibrium suggests a predominantly local mechanism. However, a local mechanism should not cause an increase in soil moisture at equilibrium, since it simply recycles the same water faster, rather than adding new water. In addition, early in the simulation, net moisture advection is quite large, suggesting a predominantly non-local mechanism early in the simulation.

3. Theory

To understand the seemingly contradictory results identified in our simulations, we introduce a conceptual model of the coupled land-atmosphere system and its response to an albedo anomaly. The intent of the conceptual model is to highlight the most essential mechanisms that cause a precipitation anomaly to arise from the surface albedo anomaly (it is not intended to be used for forecasting purposes). In particular, the conceptual model will help assess the relative importance of the local and non-local mechanisms summarized in the introduction. Full details of the derivation and justifications for relevant approximations are provided in Supporting Information S1 (Figure S4 in Supporting Information S1), with the main steps briefly summarized here. Specifically, we combine the atmospheric and soil moisture budgets (Equations S5 and S11 in Supporting Information S1), a "bucket" model for evaporation (Equation S7 in Supporting Information S1; Manabe, 1969; Seneviratne et al., 2010; Cioni and Hohenegger, 2018; Cheng et al., 2021), a simple mesoscale circulation model (Equation S8 in Supporting Information S1; Cioni and Hohenegger, 2018; Cheng et al., 2021), and a simple seepage model (Equation S9 in Supporting Information S1; Laio et al., 2001); assume anomalies in net radiation are dominated by anomalies in shortwave radiation, and that effects of anomalous cloud albedo are negligible; and approximate the land surface as a zero heat capacity surface with low permeability at the base of the surface soil layer.

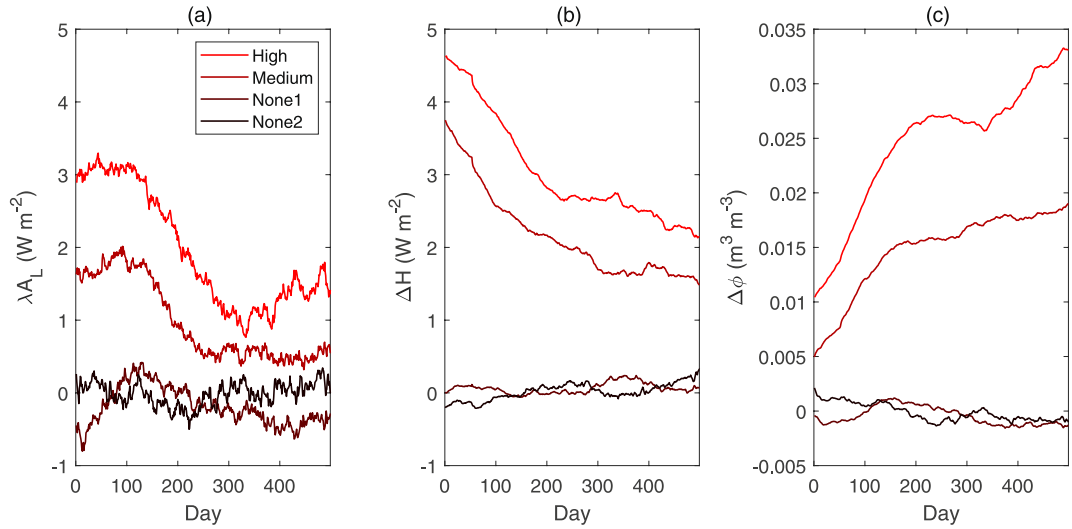

Figure 4. Temporal series (smoothed with a moving-average window of 100 days) of ensemble-averaged (a) net moisture advection (λA_L) into the low albedo anomaly, (b) sensible heat anomaly ΔH, and (c) soil moisture anomaly $\Delta\phi$ in simulations prescribed with different albedo gradients. The results from different albedo experiments are shown, following the naming convention listed in Table S1 in Supporting Information S1. "High" denotes the experiment where the prescribed visible albedo of soil in the two parts of the domain are 0.1425 and 0.0356, respectively. "Medium" denotes the experiment where the prescribed visible albedo of soil in the two parts of the domain are 0.1425 and 0.0713, respectively. "None1" ("None2") denotes the experiment where the prescribed visible albedo of soil in the two parts of the domain are both 0.1425 (0.1069).

3.1. Predicted Equilibrium Hydrologic Response to Albedo Anomalies

In its simplest form (Equations S21–S25 in Supporting Information S1), the theory predicts that, at equilibrium, fractional increases in soil moisture are proportional to fractional increases in co-albedo. Specifically, it predicts

$$\frac{\langle \Delta\phi \rangle}{\langle \phi_M \rangle} \propto \frac{\Delta a}{a_M}, \tag{1}$$

where $\Delta\phi = \phi_L - \phi_H$ is the top 1-cm soil moisture anomaly, ϕ_L is soil moisture at the lower albedo surface, ϕ_H is soil moisture at the higher albedo surface, ϕ_M is the average soil moisture across the entire domain, $a = 1 - \alpha$ is the co-albedo, α is the surface albedo, a_M is the mean co-albedo over the whole domain, and $\langle \cdot \rangle$ denotes long-term temporal averaging (see Equation S21 and associated text in Supporting Information S1).

Since the (co-)albedo anomaly is fixed in our simulations, and soil moisture is initially spatially uniform, this implies that the soil moisture anomaly is *caused* by the prescribed surface albedo anomaly. How? The atmosphere is a turbulent fluid, which turbulently diffuses water vapor downgradient; this transport mechanism efficiently smooths out horizontal gradients in water vapor. No equivalent mechanism exists in the land surface, since it is a solid rather than a turbulent fluid. Thus, the atmosphere is "well-mixed" compared to the land surface. In Supporting Information S1, we use this difference between the land and atmosphere, combined with the conceptual model, to derive the relation (see derivation of Equation S25 in Supporting Information S1):

$$\Delta\phi(t) \approx \frac{2}{h} \int_0^t A_L(\tau) d\tau, \tag{2}$$

where h is the top soil layer depth, and t is time. Thus, the soil moisture anomaly arises due to the time-integrated net advection of moisture, primarily resulting from the mesoscale circulation, which itself is driven by differential heating caused by the albedo anomaly. Thus, only the non-local mechanism is capable of generating a soil moisture anomaly; the local mechanism, in which $A_L(t) = 0$ for all t, results in no soil moisture anomaly.

In its simplest form (Equations S21–S25 in Supporting Information S1), the theory also predicts that, at equilibrium, all of the additional net radiation at the low-albedo anomaly land surface is used for evaporation, which is locally recycled back into additional precipitation over the low-albedo anomaly. Since all the additional radiation is used up by evaporation, this implies that there is no additional energy left for additional sensible heating.

Thus, there is no differential heating between the low-albedo anomaly and the surrounding region, which further implies that there is no net moisture transport by mesoscale circulations, at equilibrium. This might appear to contradict our earlier finding that mesoscale circulations cause the observed soil moisture gradient. However, there is no contradiction: the soil moisture gradient is dependent on the full history of $A_L(t)$ (Equation 2), not just the value at equilibrium ($\langle A_L \rangle$). Since mesoscale circulations exist early in the simulations, this explains how the soil moisture gradient arises in the first place.

To summarize, in its simplest form, the theory predicts that a surface albedo anomaly induces differential heating, which triggers mesoscale circulations. The circulations cause net moisture advection, increased precipitation and increased soil moisture at the low-albedo land surface anomaly. However, the resulting soil moisture anomaly increases with time, steadily reducing sensible heating at the low-albedo anomaly, and weakening the heating differential that drives the mesoscale circulation. After a sufficiently long period of time, the soil moisture anomaly is large enough to substantially weaken the heating differential and the net moisture transport from the mesoscale circulation effectively disappears, at least to first order.

3.2. Comparison With Simulations

How accurate are these predictions when compared with our cloud-permitting simulations? Quite accurate, particularly when second-order differences between the simplest version of the conceptual model and the numerical simulations are taken into account. In particular:

- The simplest version of the conceptual model (Equations S21–S25 in Supporting Information S1) assumes the soil water reservoir that controls evaporation behaves like a single "bucket", with no outflows other than evaporation, implying that the vertical seepage anomaly from the top soil layer is zero ($\Delta Q = 0$). In our simulations, soil water varies with depth, with evaporation most sensitive to the uppermost soil layers. Thus, we set the "bucket" to be the same depth as the uppermost soil layer in the model (1 cm); but this implies that some water drains to deeper layers, and thus ΔQ is non-zero. We include the effects of non-zero ΔQ using the general version (Equations S15–S18 in Supporting Information S1) of the conceptual model presented in Supporting Information S1.
- The simplest version of the conceptual model (Equations S21–S25 in Supporting Information S1) assumes the land surface has zero heat capacity, implying $\Delta G = 0$, where ΔG is the difference in ground heat fluxes between the two patches. In our simulations, ΔG is small but non-zero. We include the effects of non-zero ΔG using the general version (Equations S15–S18 in Supporting Information S1) of the conceptual model presented in Supporting Information S1.
- The simplest version of the conceptual model (Equations S21–S25 in Supporting Information S1) assumes that mesoscale circulations caused by a heating differential are the only cause of moisture advection. In fact, cold pools—density currents caused by cooling from re-evaporation of falling hydrometeors—also can contribute (Rieck et al., 2015). To evaluate the sensitivity of our results to the presence of cold pools, we include results from simulations in which cold pools have been removed (Figures 3b, 3d, 3f, and 3h), using the same approach as in Rieck et al. (2015) (see Supporting Information S1: Numerical simulations).

With these modifications, the general version of the conceptual model (Equations S15–S18 in Supporting Information S1) is compared with outputs from our cloud-permitting simulations (Figure 3). The conceptual model provides excellent estimates of $\langle \Delta H \rangle$, $\langle \lambda \Delta E \rangle$ (where λ is the latent heat of vapourization of water), and $\langle \Delta P \rangle$ across a range of albedo anomalies, both with cold pools retained (Figures 3c, 3e, and 3g, respectively), and excluded (Figures 3d, 3f, and 3h). The conceptual model estimates of $\langle A_L \rangle$ are reasonable, although biased a little low when the albedo anomaly is largest (Figure 3c). The bias is largely eliminated when cold pools are suppressed (Figure 3d), consistent with the idea that cold pools contribute to advection in the simulations, albeit to a lesser extent than the mesoscale circulation. The conceptual model provides qualitatively accurate estimates of $\langle \Delta \phi \rangle$, albeit biased low when the albedo anomaly is largest (Figure 3a). The bias essentially disappears when cold pools are suppressed (Figure 3b). This is consistent with the fact that the conceptual model neglects cold pools, which biases $\langle A_L \rangle$ low. Since $\Delta \phi(t)$ is proportional to the time integral of $A_L(t)$ (Equation 2), the negative biases in $A_L(t)$ accumulate with time, resulting in a negative bias in $\langle \Delta \phi \rangle$ that is proportionally larger than that in $\langle A_L \rangle$. Nevertheless, the conceptual model captures the most important qualitative response of $\langle \Delta \phi \rangle$ to an albedo anomaly: as the albedo anomaly increases, so does the soil moisture gradient. Thus, cold pools are not a first-order contributor to the main phenomena we seek to explain. Since the intent of the conceptual model is to explain the most important

features of the simulations with a minimum of complexity, and including cold pools in the conceptual model would significantly increase its complexity, we do not attempt to include cold pools in the conceptual model.

4. Summary and Discussion

This study has sought to understand the key mechanisms by which a land surface albedo anomaly influences precipitation at equilibrium, in the absence of other confounding anomalies in other land surface properties, such as surface roughness or vegetation. In particular, we asked: is the response dominated by a local moisture recycling mechanism, or by a non-local mesoscale circulation mechanism? Our main conclusions are as follows:

- In contrast to previous studies, which examined the transient response (Chagnon & Bras, 2005; Negri et al., 2004; Taylor et al., 2022; Wang et al., 2000), we examined the equilibrium response. We found that the equilibrium response is a hybrid of both the local and non-local mechanisms (Figure 1c): there is only limited net moisture transport by mesoscale circulations, which is characteristic of the local mechanism (Figure 1a), but a soil moisture anomaly forms, which is characteristic of the non-local mechanism (Figure 1b). To first-order, fractional increases in soil moisture are proportional to fractional increases in co-albedo (Equation 1).
- This apparent contradiction is due to the fact that the non-local mechanism dominates early in the simulation, creating a soil moisture anomaly. The soil moisture anomaly weakens the heating differential driving the non-local mesoscale circulation. At equilibrium, the heating anomaly caused by the soil moisture anomaly grows large enough to substantially reduce the heating anomaly caused by the albedo anomaly, and thus also substantially reduces the net moisture advection. In other words, at equilibrium, anomalously darker land surfaces are wetter, due to past mesoscale circulations.

Our analysis is subject to several limitations. We have examined the equilibrium response of precipitation to an albedo anomaly, but that response is inevitably sensitive to our parameterization of the large-scale atmospheric dynamics. For maximum simplicity, we consider the case with zero horizontal mean wind. The interaction between convection and large-scale forcing is parameterized in our simulations by the weak temperature gradient (WTG) approximation (Sobel et al., 2001), which is most appropriate to the tropics. The total amount of precipitation in our simulations is sensitive to the choice of reference profile used in the WTG scheme, although this sensitivity is partly mitigated by our focus on anomalies, rather than absolute values, of precipitation and soil moisture. Our results are, therefore, most representative of a wet, tropical environment with little wind. Future studies should investigate the sensitivity of our results to varying these aspects of the simulations. Our simulations are also deliberately idealized, which makes their comparison with real-world observations difficult, particularly since anomalously high soil moisture is often a cause of anomalously high vegetation density. Thus, simple comparisons between satellite observations of surface albedo and soil moisture are likely to be confounded by differences in vegetation. Although soil albedo typically decreases as soil moisture increases (Idso et al., 1975), our study deliberately neglects the influence of soil moisture on soil albedo to isolate the effects of albedo alone. Since increases in soil moisture typically result in decreases in soil albedo, and we find that a low albedo anomaly results in increased soil moisture, we would expect that including the direct effect of soil moisture on soil albedo would only amplify the mechanism identified here. Our simulations focus on soil albedo in two broad spectral bands (the photosynthetically active radiation band and the near infrared band), as is conventional, but that approximation may lead to biases in the net surface radiative forcing (Braghiere et al., 2023). Nevertheless, the hybrid mechanism we identify for the equilibrium response of precipitation to an albedo anomaly is relatively simple, providing some degree of confidence that it is robust.

This work has important implications for local geoengineering based on albedo modification. First, if albedo is deliberately increased in some region on spatial scales of $O(10\text{ km})$ to reduce local temperatures, it may increase soil moisture in the surrounding area in proportion to the albedo anomaly, reducing the heating differential between the two regions. The surrounding region will be cooler than it would be otherwise in the absence of the albedo anomaly. This "cooling halo" surrounding the modified region would be an added benefit of local radiative management. Second, if albedo must be decreased in some region on spatial scales of $O(10\text{ km})$—due to local land-use priorities unrelated to reducing local temperatures—long-term average temperature increases in that region may be mitigated by the mechanism identified here. Our results suggest that the region may attract more rainfall to supply reservoirs of water in the soil, which would cool the region, counterbalancing the increase in temperatures caused by decreased albedo. Many questions remain about the magnitude and spatial extent of such effects, which will be further investigated in future studies.

Finally, we note that LRM, like any geoengineering approach, is an imperfect and partial solution to the problem of global warming. Its potential cooling benefits are confined to a relatively small region, and may not be cost effective. If established, the albedo anomaly would need to be maintained indefinitely to avoid "termination shock," the rapid rebounding of temperatures to values they would have reached in the absence of geoengineering. Rapid increases in temperature following a termination shock may arguably be worse for local populations and ecosystems than the slower increase that would occur in the absence of geoengineering. The most direct and effective response to global warming is to reduce greenhouse gas emissions. Yet, it still seems prudent to research and understand approaches such as LRM, should global emissions reductions remain insufficient to prevent dangerous warming.

Data Availability Statement

The data set used for this study is available for public access at Harvard dataverse (https://doi.org/10.7910/DVN/WIEGH7).

Acknowledgments
K.A.M. acknowledges funding from NSF Grant AGS-2129576, the Dean's Competitive Fund for Promising Scholarship from Harvard University, and a Sloan Research Fellowship. We thank Dr. Marat Khairoutdinov for providing the models used in this study (SAM and SLM). The computations in this paper were run on the FASRC Cannon cluster supported by the FAS Division of Science Research Computing Group at Harvard University.

References

Abbott, T. H., & Cronin, T. W. (2021). Aerosol invigoration of atmospheric convection through increases in humidity. *Science*, *371*(6524), 83–85. https://doi.org/10.1126/science.abc5181

Anber, U., Gentine, P., Wang, S., & Sobel, A. H. (2015). Fog and rain in the amazon. *Proceedings of the National Academy of Sciences of the United States of America*, *112*(37), 11473–11477. https://doi.org/10.1073/pnas.150507711

Betts, A. K., & Silva Dias, M. F. (1979). Unsaturated downdraft thermodynamics in cumulonimbus. *Journal of the Atmospheric Sciences*, *36*(6), 1061–1071. https://doi.org/10.1175/1520-0469(1979)036<1061:UDTIC>2.0.CO;2

Braghiere, R., Wang, Y., Gagné-Landmann, A., Brodrick, P., Bloom, A., Norton, A., et al. (2023). The importance of hyperspectral soil albedo information for improving earth system model projections. *AGU Advances*, *4*(4), e2023AV000910. https://doi.org/10.1029/2023AV000910

Chagnon, F., & Bras, R. (2005). Contemporary climate change in the amazon. *Geophysical Research Letters*, *32*(13), L13703. https://doi.org/10.1029/2005GL022722

Charney, J. (1975). Dynamics of deserts and drought in the Sahel. *Quarterly Journal of the Royal Meteorological Society*, *101*(428), 193–202. https://doi.org/10.1002/qj.49710142802

Charney, J., Quirk, W. J., Chow, S.-H., & Kornfield, J. (1977). A comparative study of the effects of albedo change on drought in semi–arid regions. *Journal of the Atmospheric Sciences*, *34*(9), 1366–1385. https://doi.org/10.1175/1520-0469(1977)034<1366:ACSOTE>2.0.CO;2

Cheng, Y., Chan, P. W., Wei, X., Hu, Z., Kuang, Z., & McColl, K. A. (2021). Soil moisture control of precipitation re-evaporation over a heterogeneous land surface. *Journal of the Atmospheric Sciences*, *78*(10), 3369–3383. https://doi.org/10.1175/JAS-D-21-0059.1

Cheng, Y., & McColl, K. A. (2023). Thermally direct mesoscale circulations caused by land surface roughness anomalies. *Geophysical Research Letters*, *50*(16), e2023GL105150. https://doi.org/10.1029/2023GL105150

Cioni, G., & Hohenegger, C. (2018). A simplified model of precipitation enhancement over a heterogeneous surface. *Hydrology and Earth System Sciences*, *22*(6), 3197–3212. https://doi.org/10.5194/hess-22-3197-2018

Davin, E. L., & Noblet-Ducoudré, N. D. (2010). Climatic impact of global-scale deforestation: Radiative versus nonradiative processes. *Journal of Climate*, *23*(1), 97–112. https://doi.org/10.1175/2009JCLI3102.1

Davin, E. L., Seneviratne, S. I., Ciais, P., Olioso, A., & Wang, T. (2014). Preferential cooling of hot extremes from cropland albedo management. *Proceedings of the National Academy of Sciences of the United States of America*, *111*(27), 9757–9761. https://doi.org/10.1073/pnas.1317323111

Devaraju, N., Bala, G., & Modak, A. (2015). Effects of large-scale deforestation on precipitation in the monsoon regions: Remote versus local effects. *Proceedings of the National Academy of Sciences of the United States of America*, *112*(11), 3257–3262. https://doi.org/10.1073/pnas.1423439112

Evans, J. P., Meng, X., & McCabe, M. F. (2017). Land surface albedo and vegetation feedbacks enhanced the millennium drought in South-East Australia. *Hydrology and Earth System Sciences*, *21*(1), 409–422. https://doi.org/10.5194/hess-21-409-2017

Genesio, L., Bassi, R., & Miglietta, F. (2021). Plants with less chlorophyll: A global change perspective. *Global Change Biology*, *27*(5), 959–967. https://doi.org/10.1111/gcb.15470

Hales, K., Neelin, J. D., & Zeng, N. (2004). Sensitivity of tropical land climate to leaf area index: Role of surface conductance versus albedo. *Journal of Climate*, *17*(7), 1459–1473. https://doi.org/10.1175/1520-0442(2004)017<1459:SOTLCT>2.0.CO;2

Hartley, A. J., Parker, D. J., Garcia-Carreras, L., & Webster, S. (2016). Simulation of vegetation feedbacks on local and regional scale precipitation in West Africa. *Agricultural and Forest Meteorology*, *222*, 59–70. https://doi.org/10.1016/j.agrformet.2016.03.001

Idso, S., Jackson, R., Reginato, R., Kimball, B., & Nakayama, F. (1975). The dependence of bare soil albedo on soil water content. *Journal of Applied Meteorology*, *14*(1), 109–113. https://doi.org/10.1175/1520-0450(1975)014<0109:TDOBSA>2.0.CO;2

Khairoutdinov, M. F., & Randall, D. A. (2003). Cloud resolving modeling of the arm summer 1997 IOP: Model formulation, results, uncertainties, and sensitivities. *Journal of the Atmospheric Sciences*, *60*(4), 607–625. https://doi.org/10.1175/1520-0469(2003)060<0607:CRMOTA>2.0.CO;2

Khanna, J., & Medvigy, D. (2014). Strong control of surface roughness variations on the simulated dry season regional atmospheric response to contemporary deforestation in Rondônia, Brazil. *Journal of Geophysical Research: Atmospheres*, *119*(23), 13–067. https://doi.org/10.1002/2014JD022278

Kiehl, J., Hack, J., Bonan, G., Boville, B., Williamson, D., & Rasch, P. (1998). The national center for atmospheric research community climate model: CCM3. *Journal of Climate*, *11*(6), 1131–1149. https://doi.org/10.1175/1520-0442(1998)011<1131:TNCFAR>2.0.CO;2

Laguë, M. M., Bonan, G. B., & Swann, A. L. S. (2019). Separating the impact of individual land surface properties on the terrestrial surface energy budget in both the coupled and uncoupled land–atmosphere system. *Journal of Climate*, *32*(18), 5725–5744. https://doi.org/10.1175/JCLI-D-18-0812.1

Laio, F., Porporato, A., Ridolfi, L., & Rodriguez-Iturbe, I. (2001). Plants in water-controlled ecosystems: Active role in hydrologic processes and response to water stress: Ii. Probabilistic soil moisture dynamics. *Advances in Water Resources*, *24*(7), 707–723. https://doi.org/10.1016/S0309-1708(01)00005-7

Lee, J. M., & Khairoutdinov, M. (2015). A simplified land model (SLM) for use in cloud-resolving models: Formulation and evaluation. *Journal of Advances in Modeling Earth Systems*, *7*(3), 1368–1392. https://doi.org/10.1002/2014MS000419

Li, Y., Kalnay, E., Motesharrei, S., Rivas, J., Kucharski, F., Kirk-Davidoff, D., et al. (2018). Climate model shows large-scale wind and solar farms in the Sahara increase rain and vegetation. *Science*, *361*(6406), 1019–1022. https://doi.org/10.1126/science.aar5629

Manabe, S. (1969). Climate and the ocean circulation I. the atmospheric circulation and the hydrology of the Earth's surface. *Monthly Weather Review*, *97*(11), 739–774. https://doi.org/10.1175/1520-0493(1969)097<0739:CATOC>2.3.CO;2

Mostamandi, S., Predybaylo, E., Osipov, S., Zolina, O., Gulev, S., Parajuli, S., & Stenchikov, G. (2022). Sea breeze geoengineering to increase rainfall over the Arabian red sea coastal plains. *Journal of Hydrometeorology*, *23*(1), 3–24. https://doi.org/10.1175/JHM-D-20-0266.1

Negri, A. J., Adler, R. F., Xu, L., & Surratt, J. (2004). The impact of amazonian deforestation on dry season rainfall. *Journal of Climate*, *17*(6), 1306–1319. https://doi.org/10.1175/1520-0442(2004)017<1306:TIOADO>2.0.CO;2

Oleson, K. W., Bonan, G. B., & Feddema, J. (2010). Effects of white roofs on urban temperature in a global climate model. *Geophysical Research Letters*, *37*(3), L03701. https://doi.org/10.1029/2009GL042194

Ouyang, Z., Sciusco, P., Jiao, T., Feron, S., Lei, C., Li, F., et al. (2022). Albedo changes caused by future urbanization contribute to global warming. *Nature Communications*, *13*(1), 1–9. https://doi.org/10.1038/s41467-022-31558-z

Physick, W., & Tapper, N. (1990). A numerical study of circulations induced by a dry salt lake. *Monthly Weather Review*, *118*(5), 1029–1042. https://doi.org/10.1175/1520-0493(1990)118<1029:ANSOCI>2.0.CO;2

Pielke, R. A., Rodriguez, J. H., Eastman, J. L., Walko, R. L., & Stocker, R. A. (1993). Influence of Albedo variability in complex terrain on mesoscale systems. *Journal of Climate*, *6*(9), 1798–1806. https://doi.org/10.1175/1520-0442(1993)006<1798:IOAVIC>2.0.CO;2

Raymond, D. J., & Zeng, X. (2005). Modelling tropical atmospheric convection in the context of the weak temperature gradient approximation. *Quarterly Journal of the Royal Meteorological Society*, *131*(608), 1301–1320. https://doi.org/10.1256/qj.03.97

Rieck, M., Hohenegger, C., & Gentine, P. (2015). The effect of moist convection on thermally induced mesoscale circulations. *Quarterly Journal of the Royal Meteorological Society*, *141*(691), 2418–2428. https://doi.org/10.1002/qj.2532

Roy, S. B. (2009). Mesoscale vegetation-atmosphere feedbacks in Amazonia. *Journal of Geophysical Research*, *114*(D20), D20111. https://doi.org/10.1029/2009JD012001

Samuelsson, P., & Tjernström, M. (2001). Mesoscale flow modification induced by land-lake surface temperature and roughness differences. *Journal of Geophysical Research*, *106*(D12), 12419–12435. https://doi.org/10.1029/2001JD900057

Segal, M., & Arritt, R. (1992). Nonclassical mesoscale circulations caused by surface sensible heat-flux gradients. *Bulletin of the American Meteorological Society*, *73*(10), 1593–1604. https://doi.org/10.1175/1520-0477(1992)073<1593:NMCCBS>2.0.CO;2

Seneviratne, S. I., Corti, T., Davin, E. L., Hirschi, M., Jaeger, E. B., Lehner, I., et al. (2010). Investigating soil moisture–climate interactions in a changing climate: A review. *Earth-Science Reviews*, *99*(3–4), 125–161. https://doi.org/10.1016/j.earscirev.2010.02.004

Seneviratne, S. I., Phipps, S. J., Pitman, A. J., Hirsch, A. L., Davin, E. L., Donat, M. G., et al. (2018). Land radiative management as contributor to regional-scale climate adaptation and mitigation. *Nature Geoscience*, *11*(2), 88–96. https://doi.org/10.1038/s41561-017-0057-5

Sessions, S. L., Sugaya, S., Raymond, D. J., & Sobel, A. H. (2010). Multiple equilibria in a cloud-resolving model using the weak temperature gradient approximation. *Journal of Geophysical Research*, *115*(D12), D12110. https://doi.org/10.1029/2009JD013376

Sharma, A., Conry, P., Fernando, H., Hamlet, A. F., Hellmann, J., & Chen, F. (2016). Green and cool roofs to mitigate urban heat island effects in the Chicago metropolitan area: Evaluation with a regional climate model. *Environmental Research Letters*, *11*(6), 064004. https://doi.org/10.1088/1748-9326/11/6/064004

Sobel, A. H., Bellon, G., & Bacmeister, J. (2007). Multiple equilibria in a single-column model of the tropical atmosphere. *Geophysical Research Letters*, *34*(22), L22804. https://doi.org/10.1029/2007GL031320

Sobel, A. H., Nilsson, J., & Polvani, L. M. (2001). The weak temperature gradient approximation and balanced tropical moisture waves. *Journal of the Atmospheric Sciences*, *58*(23), 3650–3665. https://doi.org/10.1175/1520-0469(2001)058<3650:TWTGAA>2.0.CO;2

Spracklen, D., Baker, J., Garcia-Carreras, L., & Marsham, J. (2018). The effects of tropical vegetation on rainfall. *Annual Review of Environment and Resources*, *43*(1), 193–218. https://doi.org/10.1146/annurev-environ-102017-030136

Tang, S., Vlug, A., Piao, S., Li, F., Wang, T., Krinner, G., et al. (2023). Regional and tele-connected impacts of the Tibetan Plateau surface darkening. *Nature Communications*, *14*(1), 32. https://doi.org/10.1038/s41467-022-35672-w

Tapper, N. (1991). Evidence for a mesoscale thermal circulation over dry salt lakes. *Palaeogeography, Palaeoclimatology, Palaeoecology*, *84*(1–4), 259–269. https://doi.org/10.1016/0031-0182(91)90047-U

Taylor, C. M., Klein, C., Parker, D. J., Gerard, F., Semeena, V. S., Barton, E. J., & Harris, B. L. (2022). "Late-stage" deforestation enhances storm trends in coastal West Africa. *Proceedings of the National Academy of Sciences of the United States of America*, *119*(2). https://doi.org/10.1073/pnas.2109285119

Vahmani, P., Sun, F., Hall, A., & Ban-Weiss, G. (2016). Investigating the climate impacts of urbanization and the potential for cool roofs to counter future climate change in southern California. *Environmental Research Letters*, *11*(12), 124027. https://doi.org/10.1088/1748-9326/11/12/124027

Wang, J., Bras, R. L., & Eltahir, E. A. (2000). The impact of observed deforestation on the mesoscale distribution of rainfall and clouds in Amazonia. *Journal of Hydrometeorology*, *1*(3), 267–286. https://doi.org/10.1175/1525-7541(2000)001<0267:TIOODO>2.0.CO;2

Xu, Q., & Moncrieff, M. W. (1994). Density current circulations in shear flows. *Journal of the Atmospheric Sciences*, *51*(3), 434–446. https://doi.org/10.1175/1520-0469(1994)051<0434:DCCISF>2.0.CO;2

Xue, Y., & Shukla, J. (1993). The influence of land surface properties on Sahel climate. Part 1: Desertification. *Journal of Climate*, *6*(12), 2232–2245. https://doi.org/10.1175/1520-0442(1993)006<2232:TIOLSP>2.0.CO;2

Zhou, L., Dickinson, R., Tian, Y., Zeng, X., Dai, Y., Yang, Z.-L., & others (2003). Comparison of seasonal and spatial variations of albedos from moderate-resolution imaging spectroradiometer (MODIS) and common land model. *Journal of Geophysical Research*, *108*(D15), 4488. https://doi.org/10.1029/2002JD003326

Zonato, A., Martilli, A., Gutierrez, E., Chen, F., He, C., Barlage, M., et al. (2021). Exploring the effects of rooftop mitigation strategies on urban temperatures and energy consumption. *Journal of Geophysical Research: Atmospheres*, *126*(21), e2021JD035002. https://doi.org/10.1029/2021JD035002

Anomalously darker land surfaces become wetter due to mesoscale circulations

Yu Cheng[1], Zeyuan Hu[1], Kaighin A. McColl[1,2]

[1]Department of Earth and Planetary Sciences, Harvard University, Cambridge, Massachusetts, USA
[2]School of Engineering and Applied Sciences, Harvard University, Cambridge, Massachusetts, USA

Contents of this file

1 Supplementary Materials

1.1 Numerical simulations

We conduct deliberately idealized cloud-permitting simulations (the System for Atmospheric Modeling (Khairoutdinov & Randall, 2003)) in which only an albedo anomaly is present in an otherwise homogeneous domain. The National Center for Atmospheric Research (NCAR) Community Climate Model (CCM3) radiative transfer scheme is used to compute longwave and shortwave radiation (Kiehl et al., 1998). A prognostic subgrid-scale (SGS) turbulent kinetic energy budget model is used with a 1.5-order closure scheme (Khairoutdinov & Randall, 2003). A single-moment microphysics scheme (SAM1MOM) is used to predict the mixing ratios of hydrometeor species (Khairoutdinov & Randall, 2003). The domain is centered at 8°N in the tropics and is 25 km × 25 km × 22 km (Fig. S2) in the x, y (horizontal) and z (vertical) directions, respectively. The domain is periodic in both horizontal directions and is divided into two equal patches with different albedos in the x direction (Fig. S2). The horizontal resolution is 250 m. The vertical resolution varies with height: it is 30 m near the surface and 200 m near the top of the domain, respectively. The simulations start on January 1 and are run for 500 days, without a seasonal cycle (the diurnal cycle is retained). This simulation time is much longer than most comparable studies. Due to storage constraints, we did not output half-hourly averaged two-dimensional data over the full 500 day period; instead, once the 500-day simulations were complete, we ran additional 50-day simulations following the 500-day experiments in which high-frequency outputs were obtained. The land surface type is bare land (without vegetation) and homogeneous in all respects except for the prescribed albedo anomaly.

The WTG approximation has been applied extensively in previous studies of tropical climate over a limited domain (Raymond & Zeng, 2005; Sobel et al., 2007; Sessions et al., 2010; Cheng & McColl, 2023). In particular, Anber et al. (2015) showed that cloud-permitting simulations combined with the WTG approximation were relatively effective in capturing the seasonal and diurnal cycles of precipitation over the Amazon, in contrast to general circulation models (GCMs). The WTG scheme (Raymond & Zeng, 2005) relaxes the mean temperature profile toward a reference profile by imposing an advection term that is used to balance local convective and radiative heating. All the parameters for computing the WTG vertical velocity in this study are the same as those in Abbott and Cronin (2021), including the reference temperature profile.

Corresponding author: Kaighin A. McColl, kmccoll@seas.harvard.edu

Different initial soil moisture values are used to create an ensemble of simulations for a given prescribed albedo anomaly. The default visible albedo and near-infrared albedo values in SAM for bare soil are 0.19 and 0.38, respectively, based on satellite observations (Zhou et al., 2003). In SAM, the prescribed soil albedo is normally further multiplied by a wetness factor to represent moisture effects on albedo. As mentioned earlier, we would like soil albedo to remain independent of soil moisture in our simulations, and thus set the wetness factor to a constant value of 0.75 in all experiments. We note that both prescribed visible and near-infrared albedo are changed in the numerical experiments but the ratio of the two quantities remains the same. The prescribed anomalies are of comparable magnitude to those that could be created by local geoengineering approaches reviewed in the introduction (Seneviratne et al., 2018).

We seek to disentangle the effects of these two different mechanisms by performing simulations with cold pools eliminated. To eliminate cold pools, we follow the same approach as Rieck et al. (2015): separate simulations are run in which the evaporation of hydrometeors is switched off for simulations 'Medium' and 'High', which are both run with initial soil saturations of 20% and 30%. These simulations are referred to as the 'NOCP' simulations.

1.2 Convergence to equilibrium

Precipitation averaged over the whole domain (P_{M}) and over the low-albedo anomaly (P_{L}) rapidly approach a statistical equilibrium in our 500-day numerical simulations (Fig. S3a). In fact, both quantities are largely equilibrated after approximately 10 days (Fig. S3a), consistent with previous weak temperature gradient (WTG) experiments (Anber et al., 2015; Abbott & Cronin, 2021). Although the initial soil saturation (ϕ_{ini}) in the whole domain varies from 1% (corresponding to 0.0047 $\mathrm{m}^3\ \mathrm{m}^{-3}$) to 70% (0.3273 $\mathrm{m}^3\ \mathrm{m}^{-3}$), P_{M} at the end of the 500-day experiments is relatively insensitive to ϕ_{ini} (not shown). Similarly, simulations with different initial conditions converge to a relatively small range of domain-mean soil moisture values (ϕ_{M}) (Fig. S3b).

1.3 Column water anomaly budget

The budgets of total atmospheric moisture over each subdomain are used to compute the moisture advection between the two albedo patches. The moisture balance equation for a control volume over the low albedo anomaly can be written as

$$\frac{\partial W_{\mathrm{L}}}{\partial t} = E_{\mathrm{L}} - P_{\mathrm{L}} + A_{\mathrm{L}} + S_{\mathrm{WTG}}, \tag{S1}$$

where W_{L} (unit in mm) is column-integrated total moisture including vapor, liquid and solid water in the air over the low albedo anomaly, the subscript 'L' denotes the low albedo anomaly, E_{L} (unit in mm day^{-1}) and P_{L} (unit in mm day^{-1}) are averaged evaporation and precipitation rates over the low albedo anomaly, respectively, A_{L} (unit in mm day^{-1}) is the net horizontal advection of moisture into the low albedo anomaly, and S_{WTG} (unit in mm day^{-1}) is a source term due to the WTG approximation. Similarly, the moisture balance equation for the high-albedo patch can be written as

$$\frac{\partial W_{\mathrm{H}}}{\partial t} = E_{\mathrm{H}} - P_{\mathrm{H}} + A_{\mathrm{H}} + S_{\mathrm{WTG}}. \tag{S2}$$

As the domain is divided into two patches, we have

$$A_{\mathrm{H}} = -A_{\mathrm{L}}. \tag{S3}$$

We estimate daily averaged A_{L} and S_{WTG} by combining Equations S1-S3, since all other variables are available as outputs from the numerical simulations.

Based on Equations S1-S3, we obtain

$$\frac{\partial \Delta W}{\partial t} = \Delta E - \Delta P + 2A_{\mathrm{L}}, \tag{S4}$$

where $\Delta W = W_{\mathrm{L}} - W_{\mathrm{H}}$ and similarly for P and E. After reaching a statistical equilibrium, $\langle \frac{\partial \Delta W}{\partial t} \rangle \approx 0$, where $\langle \cdot \rangle$ denotes long-term temporal averaging. Thus, at equilibrium, the precipitation anomaly can be approximated by

$$\langle \Delta P \rangle \approx \langle \Delta E \rangle + 2 \langle A_{\mathrm{L}} \rangle. \tag{S5}$$

Equation S5 is reproduced in our simulations to very high accuracy, confirming that they have achieved a statistical equilibrium state (Figs. 3c, e & g).

1.4 Conceptual model

The conceptual model consists of four components: 1) a 'bucket model' for surface evaporation; 2) a linear model of moisture advection due to mesoscale circulations; 3) a power law model of seepage; and 4) the surface soil moisture budget.

1.4.1 Evaporation anomaly

We use a 'bucket model' for surface evaporation (Manabe, 1969; Cioni & Hohenegger, 2018; Cheng et al., 2021). Specifically, the latent heat flux over the low-albedo anomaly is

$$\lambda E_{\mathrm{L}} = A R_{\mathrm{n,L}} \times \begin{cases} 0, \text{ for } \phi_{\mathrm{L}} < \phi_{\mathrm{wp}} \\ \frac{\phi_{\mathrm{L}} - \phi_{\mathrm{wp}}}{\phi_{\mathrm{fc}} - \phi_{\mathrm{wp}}}, \text{ for } \phi_{\mathrm{wp}} \leq \phi_{\mathrm{L}} \leq \phi_{\mathrm{fc}} \\ 1, \text{ for } \phi_{\mathrm{L}} > \phi_{\mathrm{fc}} \end{cases} \tag{S6}$$

where λ is the latent heat of vaporization of water, E is the surface evaporation rate, ϕ_{wp} is the effective 'wilting point' soil moisture ($\mathrm{m}^3\ \mathrm{m}^{-3}$), ϕ_{fc} is the effective 'field capacity' ($\mathrm{m}^3\ \mathrm{m}^{-3}$), $R_{\mathrm{n,L}}$ is net radiation ($\mathrm{W\ m}^{-2}$) over the low-albedo anomaly, and A is a dimensionless parameter. Both field capacity and wilting point refer to a threshold in soil moisture (Seneviratne et al., 2010): the field capacity is the threshold above which water cannot be held in the soil against gravitational drainage, and is an approximate upper bound on soil moisture at sufficiently long time-scales; the wilting point is the threshold below which soil water cannot be absorbed by plants, and is an approximate lower bound on soil moisture, which we set to be $\phi_{\mathrm{wp}} = 0$, for maximum simplicity. Effective values of A and ϕ_{fc} are obtained by fitting Equation S6 to outputs from the cloud-permitting simulations, as in previous studies (Seneviratne et al., 2010; Cheng et al., 2021). Specifically, we obtain the estimates $A \approx 0.78 \pm 0.056$ and $\phi_{\mathrm{fc}} \approx 0.24 \pm 0.032\ \mathrm{m}^3\ \mathrm{m}^{-3}$ (Fig. S4a) where given confidence intervals are two standard errors. The resulting bucket model fits outputs from the cloud-permitting simulations reasonably well ($R^2 = 0.68$) and is used in the conceptual model for all experiments. In Fig. S4a, each dot represents the daily averaged value from a 500-day simulation, with varying albedo anomalies and initial soil moisture values.

We are primarily interested in the latent heat flux anomaly ($\lambda \Delta E \equiv \lambda E_{\mathrm{L}} - \lambda E_{\mathrm{H}}$), rather than the latent heat flux itself. Using the bucket model, this can be written as

$$\lambda \Delta E = A \times \begin{cases} 0, \text{ for } \phi_{\mathrm{H}} \leq \phi_{\mathrm{L}} < \phi_{\mathrm{wp}} \\ \frac{\phi_{\mathrm{M}} \Delta R_{\mathrm{n}} + \Delta\phi R_{\mathrm{n,M}} - \phi_{\mathrm{wp}} \Delta R_{\mathrm{n}}}{\phi_{\mathrm{fc}} - \phi_{\mathrm{wp}}}, \text{ for } \phi_{\mathrm{wp}} \leq \phi_{\mathrm{H}} \leq \phi_{\mathrm{L}} \leq \phi_{\mathrm{fc}} \\ \Delta R_{\mathrm{n}}, \text{ for } \phi_{\mathrm{L}} \geq \phi_{\mathrm{H}} > \phi_{\mathrm{fc}} \end{cases} \tag{S7}$$

where $\phi_{\mathrm{M}} = (\phi_{\mathrm{L}} + \phi_{\mathrm{H}})/2$, $\Delta\phi = \phi_{\mathrm{L}} - \phi_{\mathrm{H}}$, $R_{\mathrm{n,M}} = (R_{\mathrm{n,\,L}} + R_{\mathrm{n,\,H}})/2$, and $\Delta R_{\mathrm{n}} = R_{\mathrm{n,\,L}} - R_{\mathrm{n,\,H}}$.

In our simulations, the ensemble-averaged soil moisture typically lies between ϕ_{wp} and ϕ_{fc}. For simplicity, we assume that this is always true of ϕ_{L} and ϕ_{H} in Equations S6 and S7.

1.4.2 Atmospheric moisture advection

The conceptual model uses a simple model of moisture advection, in which moisture advection is dominated by mesoscale circulations caused by differential heating at the surface. Specifically, the net moisture advection towards the albedo anomaly is approximated as $A_{\mathrm{L}} \propto \Delta H$, where $\Delta H \equiv H_{\mathrm{L}} - H_{\mathrm{H}}$ and H is the surface sensible heat flux. A similar model has been used in previous studies (Cioni & Hohenegger, 2018; Cheng et al., 2021). In our simulations, mesoscale circulations are prominent in the morning, but their effects are confounded in the afternoon by the presence of cold pools caused by convective precipitation. We choose to ignore the effects of cold pools on A_{L} in our conceptual model to keep it maximally simple, although we test the impact of this approximation later by contrasting with cloud-permitting simulations in which cold pools are eliminated (NOCP simulations). Thus, in fitting the simple model for A_{L} in Fig. S4b, only morning outputs from the cloud-permitting simulations are used.

The model fits our simulation outputs reasonably well (Fig. S4b). Specifically,

$$\langle A_{\mathrm{L}} \rangle = \frac{k}{2\lambda} \langle \Delta H \rangle = \frac{k}{2\lambda} \langle \Delta R_{\mathrm{n}} - \lambda \Delta E - \Delta G \rangle, \tag{S8}$$

where k is a dimensionless parameter, ΔG is the difference in ground heat fluxes between the two patches, and $\Delta H = \Delta R_{\mathrm{n}} - \lambda \Delta E - \Delta G$ comes from the surface energy balance equation. We estimate $k = 13.8 \pm 1.38$, where given confidence intervals are two standard errors. The coefficient of determination is $R^2 = 0.94$.

1.4.3 Seepage anomaly

The conceptual model includes a simple model of seepage (vertical transport) of soil water. In the land surface model, soil moisture refers to the volumetric water content of the top 1 cm of soil. Following Laio et al. (2001), seepage can be approximated by a power law, $Q = K_s \phi^m$, where Q (mm day^{-1}) is seepage, K_s is soil hydraulic conductivity and m is an empirical parameter. A simple expression for the seepage anomaly $\Delta Q \equiv Q_{\mathrm{L}} - Q_{\mathrm{H}}$ is then obtained by linearizing the model for seepage around a reference $\phi = \phi_0$ that is close to ϕ_{L} and ϕ_{H}, resulting in $\Delta Q = K_s m \phi_0^{m-1} \Delta\phi + O\left((\Delta\phi)^2\right)$. Since K_s, m and ϕ_0 are constants, and $\Delta\phi$ is small, this implies that ΔQ and $\Delta\phi$ are approximately proportional to one another. Indeed, in our simulations, the relation

$$\langle \Delta Q \rangle = c \frac{(1\ \mathrm{mm})}{(1\ \mathrm{day})} \langle \Delta\phi \rangle \tag{S9}$$

fits adequately (Fig. S4c), where c is a dimensionless parameter obtained by linear regression, and 1 mm and 1 day are characteristic length and time scales that are included to make c dimensionless. Linear regression between ensemble-averaged $\langle \Delta Q \rangle$ and $\langle \Delta\phi \rangle$ results in an estimate of $c = 1.5 \pm 0.37$, where the given confidence intervals are two standard errors and the resulting $R^2 = 0.61$.

1.4.4 Surface soil moisture anomaly budget

The conceptual model uses the surface soil moisture budget to provide a governing equation for the surface soil moisture anomaly caused by the albedo anomaly. Specifically,

$$h \frac{\partial(\Delta\phi)}{\partial t} = \Delta P - \Delta E - \Delta Q, \tag{S10}$$

where h is the top soil layer depth (1 cm). There is no lateral advection of water through the top soil layer in our cloud-permitting simulations. This is by design: lateral transport of moisture through or over a flat, water-limited land surface is many orders of magnitude slower than lateral transport in the atmosphere, and ignoring it is thus a reasonable simplification here. At equilibrium, this relation reduces to

$$\langle \Delta P \rangle - \langle \Delta E \rangle - \langle \Delta Q \rangle \approx 0. \tag{S11}$$

1.4.5 Derivation of conceptual model

In this Section, we derive the conceptual model presented in the main text. We first derive a general version that is less simple but more quantitatively accurate, which is used in the comparison with cloud-permitting simulations in Fig. 3. We then highlight a special case of the general version, which is particularly simple, and highlighted in Equations 1 and 2 of the main text. First, we combine the moisture budgets (Equations S5 & S11), the bucket model for evaporation (Equation S7), the mesoscale circulation model (Equation S8) and the seepage model (Equation S9) to obtain an equation that can be solved for $\langle \Delta\phi \rangle$:

$$\langle \Delta\phi \rangle = \left\langle \left(\frac{\Delta R_\mathrm{n}}{R_\mathrm{n,M}} \left(\hat{\phi} - \phi_\mathrm{M} \right) - \frac{\phi_\mathrm{fc} - \phi_\mathrm{wp}}{A R_\mathrm{n,M}} \Delta G \right) / \left(1 + \frac{\phi_\mathrm{fc} - \phi_\mathrm{wp}}{A k R_\mathrm{n,M}} c\lambda \right) \right\rangle, \tag{S12}$$

where $\hat{\phi} \equiv \frac{1}{A}\phi_\mathrm{fc} + \left(1 - \frac{1}{A}\right)\phi_\mathrm{wp}$ and $R_\mathrm{n,M}$ is net surface radiation averaged over the whole domain. Note that $\hat{\phi}$ can be interpreted as the value of soil moisture such that $\lambda E(\hat{\phi}) = R_\mathrm{n}$, if the water-limited regime of the bucket model applied for $\phi > \phi_\mathrm{fc}$.

Second, we assume that differences in net radiation between the two albedo patches (ΔR_n) are dominated by differences in shortwave radiation (ΔR_ns), and that differences in cloud albedo are negligible. Specifically, we assume that

$$\begin{aligned} \Delta R_\mathrm{n} \approx \Delta R_\mathrm{ns} &= (1-\alpha_\mathrm{L})(1-\alpha_\mathrm{L}^c) R_\mathrm{TOA,s} - (1-\alpha_\mathrm{H})(1-\alpha_\mathrm{H}^c) R_\mathrm{TOA,s} \\ &\approx -\Delta\alpha R_\mathrm{TOA,s}, \end{aligned} \tag{S13}$$

where $R_\mathrm{TOA,s}$ is downward shortwave radiation at the top of the atmosphere, α and α^c are the land surface and cloud albedos, respectively, and $\Delta\alpha = \alpha_\mathrm{L} - \alpha_\mathrm{H}$. Similarly, the domain-averaged net radiation at the land surface can be approximated as

$$R_\mathrm{n,M} \approx (1-\alpha_\mathrm{M})(1-\alpha_\mathrm{M}^c) R_\mathrm{TOA,s} \approx (1-\alpha_\mathrm{M}) R_\mathrm{TOA,s}. \tag{S14}$$

While these two approximations both lead to biased estimates of ΔR_n and $R_\mathrm{n,M}$, we are only interested in the ratio of these quantities, which is relatively unbiased in our simulations (not shown).

Substituting Equations S13 and S14 into Equation S12 and rearranging results in

$$\frac{\langle \Delta\phi \rangle}{\hat{\phi} - \langle \phi_\mathrm{M} \rangle} = \left\langle \left(\frac{\Delta a}{a_\mathrm{M}} - \frac{\phi_\mathrm{fc} - \phi_\mathrm{wp}}{A R_\mathrm{n,M} (\hat{\phi} - \phi_\mathrm{M})} \Delta G \right) / \left(1 + \frac{\phi_\mathrm{fc} - \phi_\mathrm{wp}}{A k R_\mathrm{n,M}} c\lambda \right) \right\rangle, \tag{S15}$$

where $a = 1 - \alpha$ is the co-albedo. In our simulations, the predicted $\langle \Delta\phi \rangle$ from Equation S15 is close to that predicted from Equation S12. This further supports the approximations used in the derivation of Equation S15. Combining Equations S5, S8, S9 and S11, we obtain the following expressions:

$$\langle \Delta H \rangle = \frac{\lambda \langle \Delta Q \rangle}{k} = \frac{c\lambda \langle \Delta\phi \rangle}{k}, \tag{S16}$$

$$\lambda \langle \Delta E \rangle = \langle \Delta R_\mathrm{n} \rangle - \frac{\lambda \langle \Delta Q \rangle}{k} = \langle \Delta R_\mathrm{n} \rangle - \frac{c\lambda \langle \Delta\phi \rangle}{k}, \tag{S17}$$

and

$$\langle \Delta P \rangle = \frac{\langle \Delta R_\mathrm{n} \rangle}{\lambda} + \left(1 - \frac{1}{k}\right) \langle \Delta Q \rangle = \frac{\langle \Delta R_\mathrm{n} \rangle}{\lambda} + c \left(1 - \frac{1}{k}\right) \langle \Delta\phi \rangle. \tag{S18}$$

Finally, combining equations S4 (the budget for the total atmospheric moisture anomaly) and S10 (the budget for the soil moisture anomaly) gives the equation

$$h\Delta\phi(t) + \int_0^t \Delta Q(\tau) d\tau + \Delta W(t) = \int_0^t 2A_\mathrm{L}(\tau) d\tau. \tag{S19}$$

Since the (turbulent, fluid) atmosphere is well-mixed compared to the (solid) land surface, we make the approximation $\Delta W(t) \ll h\Delta\phi(t) + \int_0^t \Delta Q(\tau)d\tau$, which is an excellent approximation in our numerical simulations (not shown). Thus

$$\Delta\phi(t) \approx \frac{1}{h}\int_0^t (2A_{\mathrm{L}}(\tau) - \Delta Q(\tau))d\tau. \tag{S20}$$

1.4.6 Special case: zero-heat capacity surface with impermeable lower boundary

It is clarifying to consider an idealized special case of the conceptual model. First, we assume the land surface has zero heat capacity (implying $\Delta G = 0$), a common idealization of land surfaces. Second, we assume that the top soil layer is effectively impermeable at its base (implying $c = 0$). This would be the case, for example, for a shallow soil layer positioned above an impermeable bedrock, but is less accurate when the permeable soil layer(s) extend deeper. Applying these approximations results in the following equations, corresponding to equations S15-S18 and S20, respectively:

$$\frac{\langle\Delta\phi\rangle}{\langle\phi_{\mathrm{M}}\rangle} = \left(\frac{\hat{\phi} - \langle\phi_{\mathrm{M}}\rangle}{\langle\phi_{\mathrm{M}}\rangle}\right)\frac{\Delta a}{a_{\mathrm{M}}} \propto \frac{\Delta a}{a_{\mathrm{M}}}, \tag{S21}$$

$$\langle\Delta H\rangle = 0, \tag{S22}$$

$$\lambda\langle\Delta E\rangle = \langle\Delta R_{\mathrm{n}}\rangle, \tag{S23}$$

$$\lambda\langle\Delta P\rangle = \langle\Delta R_{\mathrm{n}}\rangle, \tag{S24}$$

$$\Delta\phi(t) \approx \frac{2}{h}\int_0^t A_{\mathrm{L}}(\tau)d\tau. \tag{S25}$$

We include this special case since it cleanly demonstrates the main qualitative result: the soil moisture anomaly is proportional to the normalized albedo anomaly. However, Equations S15-S18 are used in the quantitative comparison with SAM simulations in the main text (Fig. 3), since they are a little more quantitatively accurate.

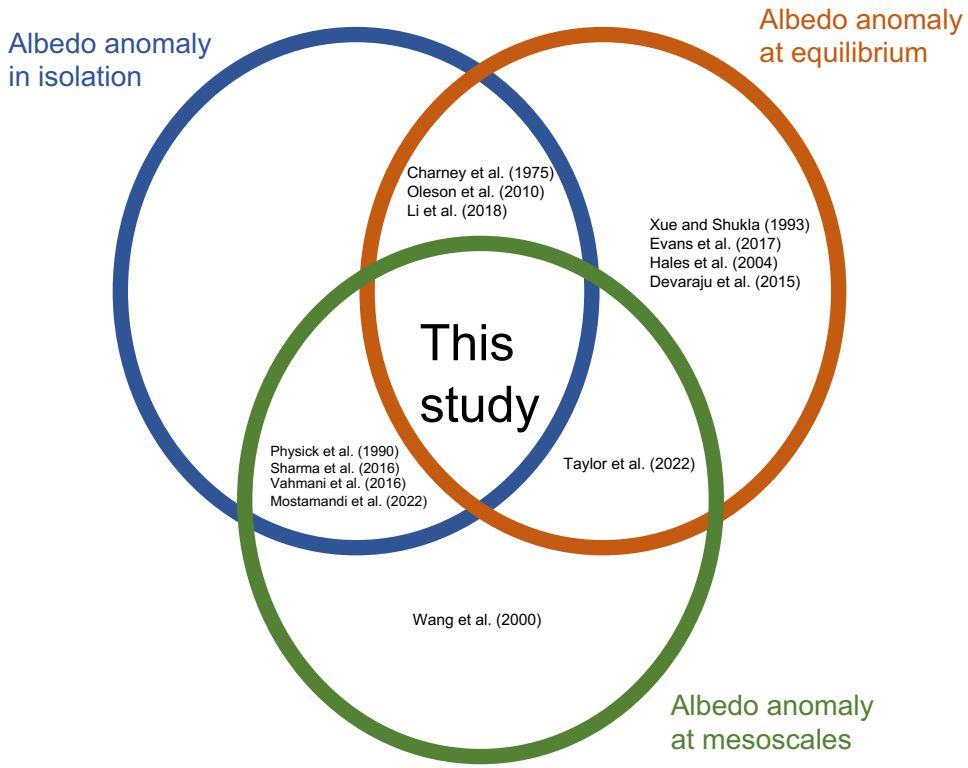

Figure S1. Venn diagram categorizing some of the previous literature (Charney, 1975; Oleson et al., 2010; Li et al., 2018; Xue & Shukla, 1993; Evans et al., 2017; Hales et al., 2004; Devaraju et al., 2015; Taylor et al., 2022; Physick & Tapper, 1990; Sharma et al., 2016; Vahmani et al., 2016; Mostamandi et al., 2022; Wang et al., 2000) investigating land surface albedo effects on climate. The main novelty of this study is its investigation of the *equilibrium* response of precipitation to *mesoscale* albedo anomalies *in isolation*.

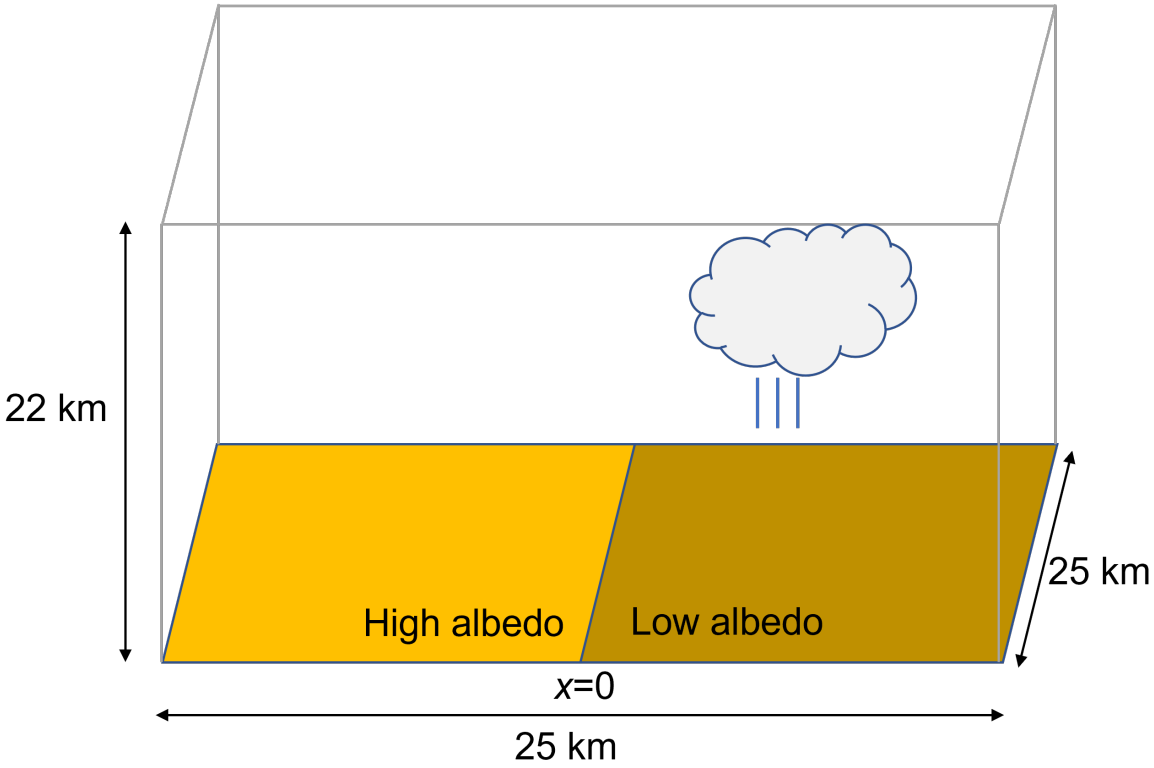

Figure S2. Schematic illustration of simulated region.

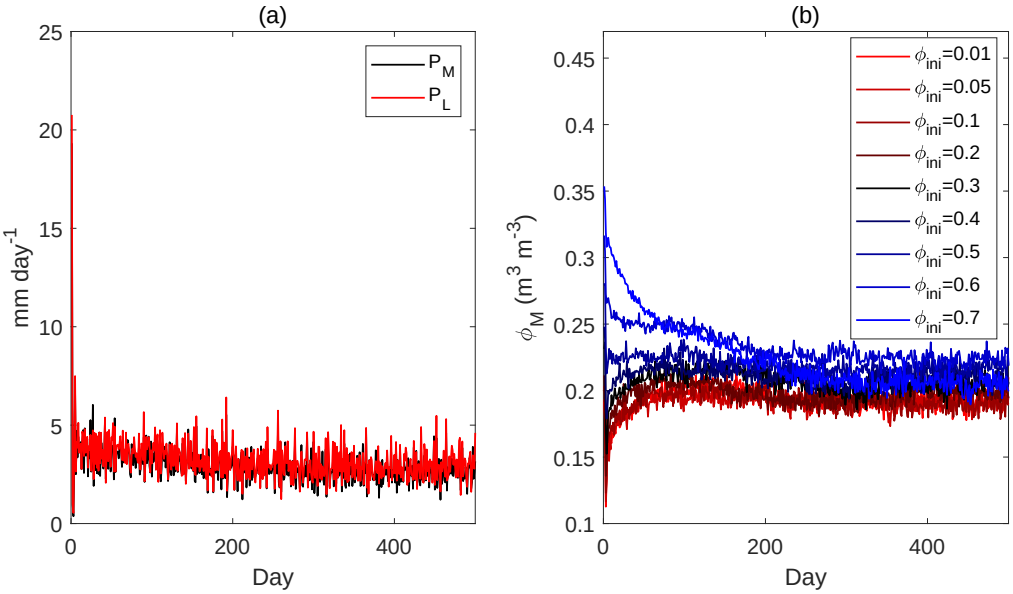

Figure S3. (a) Temporal series of daily precipitation averaged over the whole domain (P_{M}) and over the low albedo anomaly (P_{L}) in the experiment 'Medium' where the initial soil saturation is 10%. (b) Temporal series of soil moisture averaged over the whole domain (ϕ_{M}) in experiments 'Medium' prescribed with different initial soil moisture.

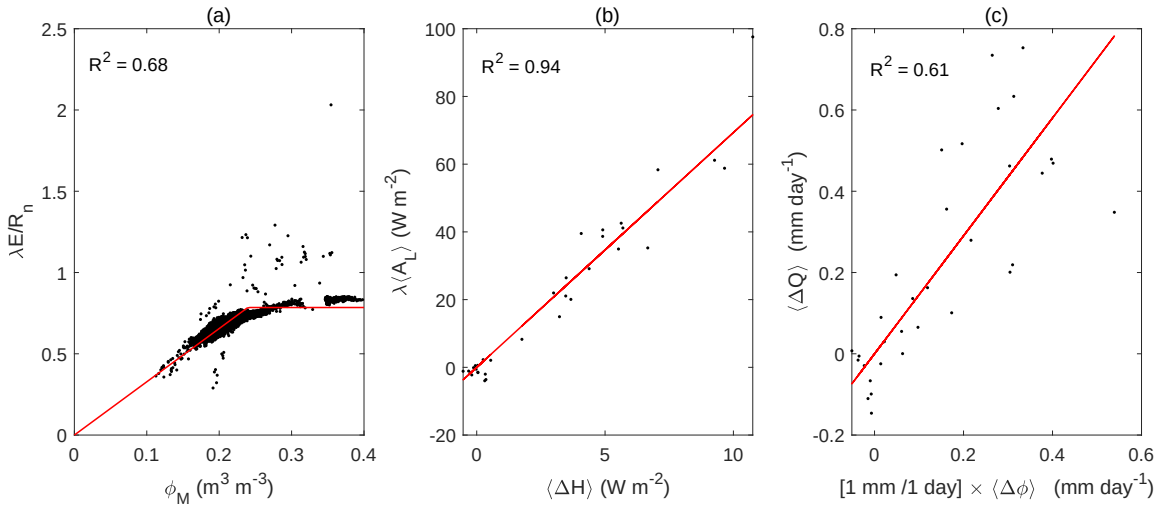

Figure S4. Fitting the conceptual model to outputs from the cloud-permitting simulations. (a) The fitted bucket model for latent heat flux based on numerical simulations. Each dot in (a) represents daily averaged values in all 500-day simulations described in Table 1. (b) The linear model for $\langle A_{\mathrm{L}} \rangle$ and $\langle \Delta H \rangle$ based on numerical simulations. (c) The linear model for $\langle \Delta Q \rangle$ and $\frac{1\ \mathrm{mm}}{1\ \mathrm{day}} \times \langle \Delta \phi \rangle$. Each dot in (b) and (c) represents the long-term average of variables in a numerical experiment described in Table 1 for morning and whole-day series, respectively.

Table S1. List of experiments run in this study. 'albedo' refers to the prescribed surface visible albedo. The same set of ϕ_{ini} are prescribed for 'Medium' and 'High'.

Numerical experiments	albedo α_{H}	albedo α_{L}	Initial soil moisture ϕ_{ini} (%) ($\mathrm{m}^3\ \mathrm{m}^{-3}$)
Medium	0.1425	0.0713	1 (0.0047), 5 (0.0234), 10 (0.0468), 20 (0.0935), 30 (0.1403), 40 (0.1870), 50 (0.2338), 60 (0.2805), 70 (0.3273)
High	0.1425	0.0356	1 (0.0047), 5 (0.0234), 10 (0.0468), 20 (0.0935), 30 (0.1403), 40 (0.1870), 50 (0.2338), 60 (0.2805), 70 (0.3273)
None1	0.1425	0.1425	10 (0.0468), 20 (0.0935), 30 (0.1403), 40 (0.1870), 50 (0.2338), 60 (0.2805)
None2	0.1069	0.1069	10 (0.0468), 20 (0.0935), 30 (0.1403), 40 (0.1870), 50 (0.2338), 60 (0.2805)
Medium_NOCP	0.1425	0.0713	20 (0.0935), 30 (0.1403)
High_NOCP	0.1425	0.0356	20 (0.0935), 30 (0.1403)

References

Abbott, T. H., & Cronin, T. W. (2021). Aerosol invigoration of atmospheric convection through increases in humidity. *Science*, *371*(6524), 83–85. https://doi.org/10.1126/science.abc5181.

Anber, U., Gentine, P., Wang, S., & Sobel, A. H. (2015). Fog and rain in the amazon. *Proc. Natl. Acad. Sci.*, *112*(37), 11473–11477. https://doi.org/10.1073/pnas.150507711.

Charney, J. (1975). Dynamics of deserts and drought in the sahel. *Quart. J. Roy. Meteor. Soc.*, *101*(428), 193–202. https://doi.org/10.1002/qj.49710142802.

Cheng, Y., Chan, P. W., Wei, X., Hu, Z., Kuang, Z., & McColl, K. A. (2021). Soil moisture control of precipitation re-evaporation over a heterogeneous land surface. *J. Atmos. Sci.*, *78*(10). https://doi.org/10.1175/JAS-D-21-0059.1.

Cheng, Y., & McColl, K. A. (2023). Thermally direct mesoscale circulations caused by land surface roughness anomalies. *Geophys. Res. Lett.*, *50*(16), e2023GL105150. https://doi.org/10.1029/2023GL105150.

Cioni, G., & Hohenegger, C. (2018). A simplified model of precipitation enhancement over a heterogeneous surface. *Hydrol. Earth Syst. Sci.*, *22*, 3197–3212. https://doi.org/10.5194/hess-22-3197-2018.

Devaraju, N., Bala, G., & Modak, A. (2015). Effects of large-scale deforestation on precipitation in the monsoon regions: Remote versus local effects.

Proc. Natl. Acad. Sci., *112*(11), 3257–3262. https://doi.org/10.1073/pnas.1423439112.

Evans, J. P., Meng, X., & McCabe, M. F. (2017). Land surface albedo and vegetation feedbacks enhanced the millennium drought in south-east australia. *Hydrol. Earth Syst. Sci.*, *21*(1), 409–422. https://doi.org/10.5194/hess-21-409-2017.

Hales, K., Neelin, J. D., & Zeng, N. (2004). Sensitivity of tropical land climate to leaf area index: Role of surface conductance versus albedo. *J. Clim.*, *17*(7), 1459 - 1473. https://doi.org/10.1175/1520-0442(2004)017<1459:SOTLCT>2.0.CO;2.

Khairoutdinov, M. F., & Randall, D. A. (2003). Cloud resolving modeling of the arm summer 1997 iop: Model formulation, results, uncertainties, and sensitivities. *J. Atmos. Sci.*, *60*(4), 607–625. https://doi.org/10.1175/1520-0469(2003)060<0607:CRMOTA>2.0.CO;2.

Kiehl, J., Hack, J., Bonan, G., Boville, B., Williamson, D., & Rasch, P. (1998). The national center for atmospheric research community climate model: Ccm3. *J. Clim.*, *11*(6), 1131–1149. https://doi.org/10.1175/1520-0442(1998)011<1131:TNCFAR>2.0.CO;2.

Laio, F., Porporato, A., Ridolfi, L., & Rodriguez-Iturbe, I. (2001). Plants in water-controlled ecosystems: active role in hydrologic processes and response to water stress: Ii. probabilistic soil moisture dynamics. *Adv. Water Resour.*, *24*(7), 707–723. https://doi.org/10.1016/S0309-1708(01)00005-7.

Li, Y., Kalnay, E., Motesharrei, S., Rivas, J., Kucharski, F., Kirk-Davidoff, D., ... Zeng, N. (2018). Climate model shows large-scale wind and solar farms in the sahara increase rain and vegetation. *Science*, *361*(6406), 1019–1022. https://doi.org/10.1126/science.aar5629.

Manabe, S. (1969). Climate and the ocean circulation i. the atmospheric circulation and the hydrology of the earth's surface. *Mon. Weather Rev.*, *97*(11), 739–774. https://doi.org/10.1175/1520-0493(1969)097<0739:CATOC>2.3.CO;2.

Mostamandi, S., Predybaylo, E., Osipov, S., Zolina, O., Gulev, S., Parajuli, S., & Stenchikov, G. (2022). Sea breeze geoengineering to increase rainfall over the arabian red sea coastal plains. *J. Hydrometeorol.*, *23*(1), 3–24. https://doi.org/10.1175/JHM-D-20-0266.1.

Oleson, K. W., Bonan, G. B., & Feddema, J. (2010). Effects of white roofs on urban temperature in a global climate model. *Geophys. Res. Lett.*, *37*(3). https://doi.org/10.1029/2009GL042194.

Physick, W., & Tapper, N. (1990). A numerical study of circulations induced by a dry salt lake. *Mon. Weather Rev.*, *118*(5), 1029–1042. https://doi.org/10.1175/1520-0493(1990)118<1029:ANSOCI>2.0.CO;2.

Raymond, D. J., & Zeng, X. (2005). Modelling tropical atmospheric convection in the context of the weak temperature gradient approximation. *Quart. J. Roy. Meteor. Soc.*, *131*(608), 1301–1320. https://doi.org/10.1256/qj.03.97.

Rieck, M., Hohenegger, C., & Gentine, P. (2015). The effect of moist convection on thermally induced mesoscale circulations. *Quart. J. Roy. Meteor. Soc.*, *141*(691), 2418–2428. https://doi.org/10.1002/qj.2532.

Seneviratne, S. I., Corti, T., Davin, E. L., Hirschi, M., Jaeger, E. B., Lehner, I., ... Teuling, A. J. (2010). Investigating soil moistureclimate interactions in a changing climate: A review. *Earth-Sci. Rev.*, *99*(3-4), 125–161. https://doi.org/10.1016/j.earscirev.2010.02.004.

Seneviratne, S. I., Phipps, S. J., Pitman, A. J., Hirsch, A. L., Davin, E. L., Donat, M. G., ... Kravitz, B. (2018). Land radiative management as contributor to regional-scale climate adaptation and mitigation. *Nat. Geosci.*, *11*, 8896. https://doi.org/10.1038/s41561-017-0057-5.

Sessions, S. L., Sugaya, S., Raymond, D. J., & Sobel, A. H. (2010). Multiple equilibria in a cloud-resolving model using the weak temperature gradient approx-

imation. *J. Geophys. Res. Atmos.*, *115*(D12). https://doi.org/10.1029/2009JD013376.

Sharma, A., Conry, P., Fernando, H., Hamlet, A. F., Hellmann, J., & Chen, F. (2016). Green and cool roofs to mitigate urban heat island effects in the chicago metropolitan area: Evaluation with a regional climate model. *Environ. Res. Lett.*, *11*(6), 064004. https://dx.doi.org/10.1088/1748-9326/11/6/064004.

Sobel, A. H., Bellon, G., & Bacmeister, J. (2007). Multiple equilibria in a single-column model of the tropical atmosphere. *Geophys. Res. Lett.*, *34*(22). https://doi.org/10.1029/2007GL031320.

Taylor, C. M., Klein, C., Parker, D. J., Gerard, F., Semeena, V. S., Barton, E. J., & Harris, B. L. (2022). late-stage deforestation enhances storm trends in coastal west africa. *Proc. Natl. Acad. Sci.*, *119*(2). https://doi.org/10.1073/pnas.2109285119.

Vahmani, P., Sun, F., Hall, A., & Ban-Weiss, G. (2016). Investigating the climate impacts of urbanization and the potential for cool roofs to counter future climate change in southern california. *Environ. Res. Lett.*, *11*(12), 124027. https://dx.doi.org/10.1088/1748-9326/11/12/124027.

Wang, J., Bras, R. L., & Eltahir, E. A. (2000). The impact of observed deforestation on the mesoscale distribution of rainfall and clouds in amazonia. *J. Hydrometeorol.*, *1*(3), 267–286. https://doi.org/10.1175/1525-7541(2000)001<0267:TIOODO>2.0.CO;2.

Xue, Y., & Shukla, J. (1993). The influence of land surface properties on sahel climate. part 1: desertification. *J. Clim.*, *6*(12), 2232–2245. https://doi.org/10.1175/1520-0442(1993)006<2232:TIOLSP>2.0.CO;2.

Zhou, L., Dickinson, R., Tian, Y., Zeng, X., Dai, Y., Yang, Z.-L., ... others (2003). Comparison of seasonal and spatial variations of albedos from moderate-resolution imaging spectroradiometer (modis) and common land model. *J. Geophys. Res. Atmos.*, *108*(D15). https://doi.org/10.1029/2002JD003326.